Received: 5 August 2021 | Revised: 9 November 2021 | Accepted: 9 November 2021

DOI: 10.1002/pro.4242

FULL-LENGTH PAPER

Two different kinds of interaction modes of deaminase APOBEC3A with single-stranded DNA in solution detected by nuclear magnetic resonance

Yaping Liu[1,2] | **Wenxian Lan**[1] | **Chunxi Wang**[1] | **Chunyang Cao**[1,2]

[1]State Key Laboratory of Bioorganic and Natural Product Chemistry, Center for Excellence in Molecular Synthesis, Shanghai Institute of Organic Chemistry, Chinese Academy of Sciences, Shanghai, China

[2]University of Chinese Academy of Science, Beijing, China

Correspondence
Chunyang Cao, State Key Laboratory of Bioorganic and Natural Product Chemistry, Center for Excellence in Molecular Synthesis, Shanghai Institute of Organic Chemistry, Chinese Academy of Sciences, 345 Lingling Road, Shanghai 200032, China.
Email: ccao@mail.sioc.ac.cn

Funding information
Center for Excellence in Molecular Synthesis, CAS, Grant/Award Number: FZHCZY020600; National Natural Science Foundation of China, Grant/Award Numbers: 21778065, 21807105, 21977110, 22174155, 22177127; National Program on Key Basic Research Project of China, Grant/Award Numbers: 2016YFA0502302, 2017YFE0108200; Strategic Priority Research Program of the Chinese Academy of Sciences, Grant/Award Number: XDB 20000000

Abstract

APOBEC3A (A3A) deaminates deoxycytidine in target motif TC in a single-stranded DNA (we termed it as TC DNA), which mortally mutates viral pathogens and immunoglobulins, and leads to the diversification and lethality of cancers. The crystal structure of A3A-DNA revealed a unique U-shaped recognition mode of target base dC_0. However, when TC DNA was titrated into ^{15}N-labeled A3A solution, we observed two sets of ^{1}H-^{15}N cross-peaks of A3A in HSQC spectra, and two sets of ^{1}H-^{1}H cross-peaks of DNA in two-dimensional ^{13}C,^{15}N-filtered TOCSY spectra, indicating two different kinds of conformers of either A3A or TC DNA existing in solution. Here, mainly by NMR, we demonstrated that one DNA conformer interacted with one A3A conformer, forming a specific complex $A3A^{S}$-DNA^{S} in a way almost similar to that observed in the reported crystal A3A-DNA structure, where dC_0 inserted into zinc ion binding center. While the other DNA conformer bound with another A3A conformer, but dC_0 did not extend into the zinc-binding pocket, forming a non-specific $A3A^{NS}$-DNA^{NS} complex. The NMR solution structure implied three sites Asn^{61}, His^{182} and Arg^{189} were necessary to DNA recognition. These observations indicate a distinctive way from that reported in X-ray crystal structure, suggesting an unexpected mode of deaminase APOBEC3A to identify target motif TC in DNA in solution.

KEYWORDS

APOBEC3A, DNA, identification, nuclear magnetic resonance, structure

1 | INTRODUCTION

APOBEC3 (A3), a family of activation-induced cytidine deaminases, contains seven members APOBEC3A (A3A), APOBEC3B (A3B), APOBEC3C (A3C), APOBEC3DE (A3DE), APOBEC3F (A3F), APOBEC3G (A3G) and APOBEC3H (A3H). They deaminate deoxycytidines into uridines in single-stranded DNA (ssDNA) during reverse transcription, which produces G to A hypermutations in a viral genome, generates defective proteins and proviruses, thus decreases the possibility of further viral replication.[1–4] A3s generally display differential substrate binding specificities (C<u>C</u> or T<u>C</u>), leading to altered frequencies of mutation of deoxycytidines.[1–3,5–8] Among them, A3DE, A3F, A3G and A3H restrict replication of HIV-1 virus in strains lacking the virus infectivity factor

Yaping Liu and Wenxian Lan contributed equally to this study.

(Vif) by deaminating cytidine in virus cDNA.[9–13] Vif facilitates polyubiquitination of A3 members, leading to proteasomal degradation.[14–19] Specifically, A3A suppresses HIV-1 primary infection in macrophages,[20,21] as well as other viruses (including hepatitis B virus, human papillomavirus, Epstein–Barr virus, cytomegalovirus, and herpes simplex virus type 1) by inducing the lethal mutation in viral genomic DNA through cytidine deamination.[21–24]

To study how A3s specifically recognize the target motifs TC or CC in DNA, many structures of A3-DNA complexes had been reported.[25,26] The structure of human A3F-CD2 (i.e., hA3F-CD2) in complex with a 10-dT ssDNA (PDB code 5W2M)[27] shows that DNA is far away from catalytic zinc-binding motif, while the structures of chimeric hA3F-CD2 (i.e., hA3Fc-CD2) in complex with DNA strands (PDB codes 5ZVA and 5ZVB) demonstrate two DNA binding sites on hA3Fc-CD2.[28] One is formed by Tyr^{333}, Lys^{358} and Tyr^{359} in one monomer of hA3Fc-CD2, the other is composed by conserved residues Trp^{277}, $Y_{307}YFW_{310}$ near to Zn^{2+} binding region in another monomer hA3Fc-CD2. The structure of inactive pseudo-catalytic *rhesus macaque* A3G-NTD (i.e., rA3G-NTD) in complex with poly-dT ssDNA (PDB code 5K83)[29] reveals that only one deoxythymidine is in a shallow cleft close to the pseudo-catalytic zinc-binding motif. The structures of A3G-CD2 in complex with two deamination product DNA strands containing 5-iodinated CUC^{I} and CCU^{I} motifs (PDB codes 6K3J and 6K3K)[30] imply the structural basis of the two DNA binding modes responsible for cytidine deamination in TCC and CCC motifs catalyzed by A3G, respectively. The 10-site A3G-CD2 variant (i.e., P200A, L234K, N236A, C243A, P247K, Q318K, F310K, C321A, Q322A, and C356A, termed as A3G-CTD2) was reported to have much stronger binding affinity to DNA and higher catalytic efficiency than wild-type A3G-CD2.[31] The structure of the inactive form A3G-CTD2 E259A variant (i.e., A3G-CTD2*) complexed with ssDNA (PDB code 6bux)[31] demonstrates that only base dC_0 in the target motif 5′-$C_{-1}C_0C_1$ inserts into the pocket of the zinc-binding active site region. Residues Asp^{316} and Asp^{317} of A3G-CTD2* form hydrogen-bonds with base dC_{-1}, accounting for their roles in identifying base dC_{-1}. The structures of inactive variant A3A E72A or E72A/C171A[32,33] (Glu^{72} is conserved in A3 family, Figure S1, Supporting Information) and chimeric A3B variant E255A-CD2[33] (i.e., A3Bctd-QMloop3A3Aloop1 or A3B-CTD*, in which loop 3 of A3B was replaced by loop 1 of A3A) in complexes with DNA (PDB codes 5KEG, 5SWW and 5TD5) also show that only cytidine in hotspot 5′-TC inserts into zinc-binding active site pocket. One molecular DNA binds to one molecular A3A or chimeric A3B-CD2 in a U-shaped mode, similar to that observed in A3G-CTD2*-DNA complex. These three structures obviously visualize the active sites poised for catalysis of A3A and A3B, and pinpoints the residues conferring the specificity of TC motif.

All those reported results indicated that A3 proteins (including A3A) identified the target base dC_0 in one mode, where the base dC_0 must insert into the active site of A3A. From this point, the specific identification of base dC_0 is in a unique way. It is well known that, by nuclear magnetic resonance (NMR) technique, the dynamic process can be sometimes observed. Thus, we decided to investigate the interactions of A3A with DNA in solution by NMR, since the assignment of the atoms ^{13}C, ^{15}N and ^{1}H of inactive A3A variant L63N/C64S/E72Q/C171Q (i.e., $A3A_{4M}$ in the current report) was accessible.[34] The residues L63, C64 and C171 are located in the surface of A3A, the mutation from L63 to N63 improves protein solubility, while the mutations C64S and C171Q are helpful to avoid A3A aggregation by forming disulfide bond between two A3A monomers, thus resolving ambiguous assignments of free A3A.[34] We made ^{15}N-labled NMR sample, and acquired ^{1}H-^{15}N HSQC spectrum, which displayed resolved cross-peaks (Figure S2), consistent with the previous observation.[34] However, during our NMR studies, we found that, upon TC DNA (with a sequence of 5′-ATTTT$_{-1}C_0A_{+1}$ATT-3′, Table 1) being titrated into the solution of ^{15}N labeled inactive $A3A_{4M}$, $A3A_{4M}$ variant two sets of ^{1}H-^{15}N cross-peak signals belonging to $A3A_{4M}$ in two-dimensional (2D) ^{1}H-^{15}N HSQC spectrum (Figure 1a) were observed even at a molar ratio less than 1:1, and two sets of ^{1}H-^{1}H correlation signals belonging to TC DNA were either found in 2D ^{13}C,^{15}N-filtered ^{1}H-^{1}H TOCSY (Figure 1b,c).

TABLE 1 5′-FAM-labeled DNA strands used in this manuscript

ssDNA	K_d (μM)	Sequence
TC	0.086 ± 0.010	5′-ATT TTC AAT T-3′
TTC-1	5.683 ± 0.236	5′-TTT CTT T-3′
TTC-2	3.486 ± 0.172	5′-TTT TCT TTT-3′
TTC-3	2.624 ± 0.070	5′-TTT TCT TTT TT-3′
TTC-4	4.280 ± 0.273	5′-TTT TCT TTT TTT T-3′
TTC-5	3.852 ± 0.294	5′-TTT TCT TTT TTT TTT-3′
TTC-6	4.193 ± 0.306	5′-TTT TCT TTT TTT TTT TT-3′
TTC-7	3.610 ± 0.091	5′-TTT TTT CTT TT-3′
TTC-8	19.925 ± 2.091	5′-TTT TTT TTC TTT T-3′
TTC-9	10.490 ± 1.104	5′-TTT TTT TTT TCT TTT-3′
TTC-10	9.188 ± 0.846	5′-TTT TTT TTT TTT CTT TT-3′
TTC-11	39.184 ± 2.524	5′-TTT TTT TTT TTT TTT TCT TTT-3′

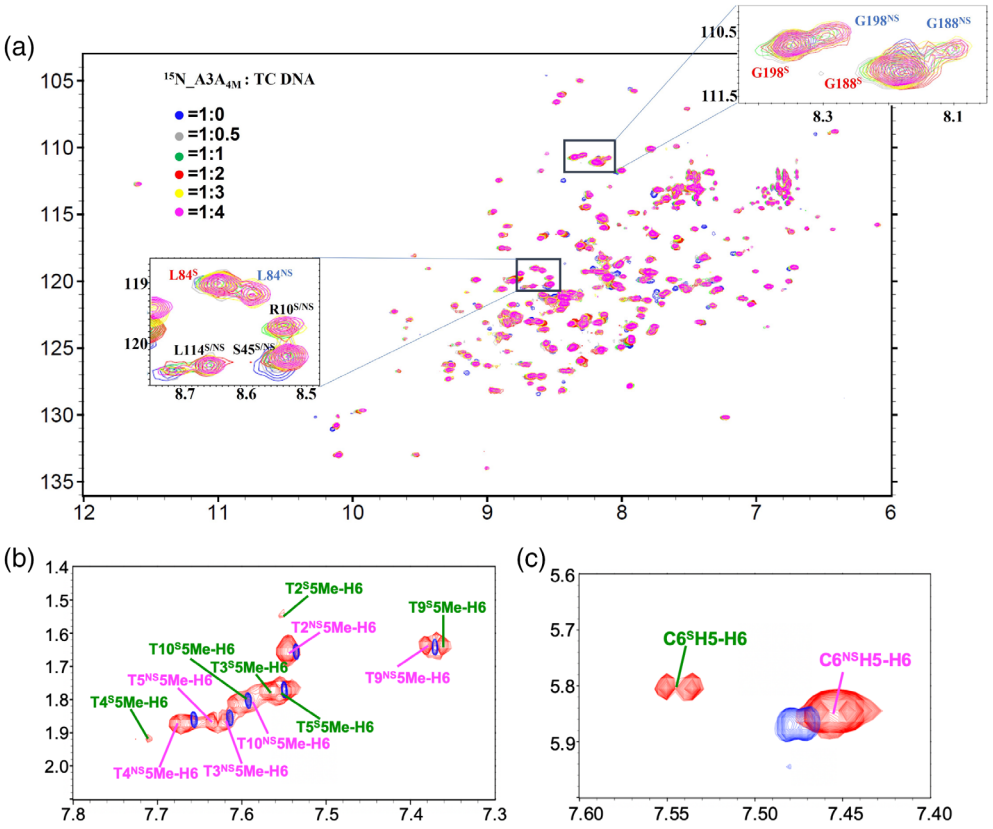

FIGURE 1 Two kinds of conformers of either A3A$_{4M}$ or TC DNA in solution upon their interaction with each other were observed by NMR technique. (a) ^{1}H-^{15}N HSQC spectra superimposition at different molar ratios of A3A$_{4M}$ versus DNA. (b) ^{13}C /^{15}N filtered two-dimensional (2D) ^{1}H-^{1}H TOCSY spectrum was overlapped with the 2D TOCSY spectrum of free TC DNA. In (b, c), the ^{1}H-^{1}H cross-peaks of free TC DNA were displayed in blue. The assignment of the signals in (a–c) indicated the residues in A3A^{S} or DNA^{S} (in green) and A3A^{NS} or DNA^{NS} (in pink)

After we finished assignment of the backbone atoms of A3A$_{4M}$, we selected several cross-peaks belonging to residues L12, V150, S187 and G198 in ^{1}H-^{15}N HSQC spectra acquired at different molar ratio, and measured the intensity ratios of these cross-peaks, the results were shown in Figure S3. From Figure S3, we can conclude that, after A3A$_{4M}$ was mixed with DNA at different molar ratios (TC DNA vs. A3A$_{4M}$), the intensity ratio of the two complexes (specific vs. nonspecific binding states) is almost unchanged. Obviously, these observations indicated that A3A$_{4M}$ interacted with TC DNA in solution in a manner, not completely identical to those observed in the reported crystal structures of A3-DNA complexes mentioned above. To account for these observations, we here conducted extensive NMR studies on the interactions between A3A$_{4M}$ and TC DNA.

2 | RESULTS AND DISCUSSION

2.1 | Two kinds of A3A$_{4M}$-DNA complexes observed in solution

To study how A3A interacted with TC DNA in solution, we first conducted extensive NMR studies on the interactions between A3A$_{4M}$ and TC DNA. We titrated TC DNA into ^{15}N-labeled A3A$_{4M}$ solution. In the absence of DNA, there is only one set of ^{1}H-^{15}N cross peaks in the HSQC spectra, although some peaks have weak intensity due to the mixed forms of monomer and dimer A3A$_{4M}$ in solution, determined by running ultracentrifugation (Figure S4). However, the addition of TC DNA into A3A$_{4M}$ solution led to two sets of ^{1}H-^{15}N cross peaks of A3A$_{4M}$ shown up in ^{1}H-^{15}N HSQC spectra, indicating that two kinds of A3A$_{4M}$ conformers existing in solution. Moreover, this observation was independent on the molar ratio of A3A$_{4M}$ versus TC DNA. When the molar ratio was increased up to 1:2, the cross-peaks did not shift any longer. So, to do NMR studies on the interactions between A3A$_{4M}$ and TC DNA, we made NMR samples of double isotope ^{13}C, ^{15}N labeled or triple isotope ^{13}C, ^{15}N, ^{2}H labeled A3A$_{4M}$ in complex with TC DNA at a molar ratio 1:2 for further NMR experiments.

To clearly identify the signals belonging to the bound TC DNA, we acquired 2D ^{1}H-^{31}P HETCOR spectrum, ^{13}C/^{15}N-filtered ^{1}H-^{1}H TOCSY and ^{1}H-^{1}H NOESY spectra. Interestingly, in the 2D filtered TOCSY spectrum (Figure 1b,c), two sets of ^{1}H-^{1}H cross-peaks of DNA were also observed, indicating that two kinds of DNA conformers existing in solution, either. Compared the chemical shifts of A3A-bound DNA with those of free DNA, we found that, in one A3A-bound TC DNA conformer, which displayed more protons displaying chemical shift changes (Figure S5a), its protons demonstrated different

intra-DNA ^{1}H-^{1}H NOE patterns from those observed in NOESY spectrum of free TC DNA. So, we tentatively named this kind of DNA conformation as A3A$_{4M}$ specifically bound conformer (i.e., DNA^{S}). In contrast, in another A3A-bound TC DNA conformer, which had fewer protons demonstrating chemical shifts changes (Figure S5b), its protons had intra-DNA ^{1}H-^{1}H NOE patterns almost similar to those observed in NOESY spectrum of free TC DNA. We thus termed this kind of TC DNA conformation as A3A$_{4M}$ nonspecifically bound conformer (i.e., DNA^{NS}). To assign NMR signals of A3A in different states, a series of 2D and three-dimensional (3D) NMR experiments were then performed to assign NMR signals belonging to backbone and side-chain atoms of A3A$_{4M}$, and intramolecular NOEs in A3A$_{4M}$ (described in section 4.1). Compared to the free A3A$_{4M}$, the chemical shifts changes of the backbone nitrogen atoms and amide protons of A3A$_{4M}$ (Figure 2) implied that the TC DNA binding regions in two kinds of A3A$_{4M}$ conformers were almost similar to each other, mainly locating in the loops 1, 3, 5 and 7. Subsequently, by analyzing 3D ^{13}C-F1 edited, ^{13}C/^{15}N-F3 filtered NOESY spectra, we got intermolecular NOEs between A3A$_{4M}$ and TC DNA. We found that one A3A$_{4M}$ conformer individually displayed intermolecular NOEs with only one TC DNA conformer. We thus termed two different kinds of A3A$_{4M}$ conformers as DNA^{S} bound A3A$_{4M}$ (i.e., A3A^{S}) and DNA^{NS} bound A3A$_{4M}$ (i.e., A3A^{NS}). To explore how DNA^{S} and DNA^{NS} interacted with A3A^{S} and A3A^{NS}, respectively, we further decided to determine the solution structures of the A3A^{NS}-DNA^{NS} and A3A^{S}-DNA^{S} complexes. So, we assigned all intramolecular NOEs in DNA^{NS}, DNA^{S}, A3A^{S} and A3A^{NS}, intermolecular NOEs between A3A^{S} and DNA^{S}, and between A3A^{NS} and DNA^{NS}.

2.2 | DNA^{S} binds A3A$_{4M}$ in a manner almost similar to that observed in the reported crystal structures of A3A-DNA or A3B-DNA complexes

To calculate NMR structures of A3A^{NS}-DNA^{NS} and A3A^{S}-DNA^{S} complexes, we generated 3,346 and 3,409 distance constraints derived from NOE intensities in total (including 50 and 95 intermolecular NOEs, which were

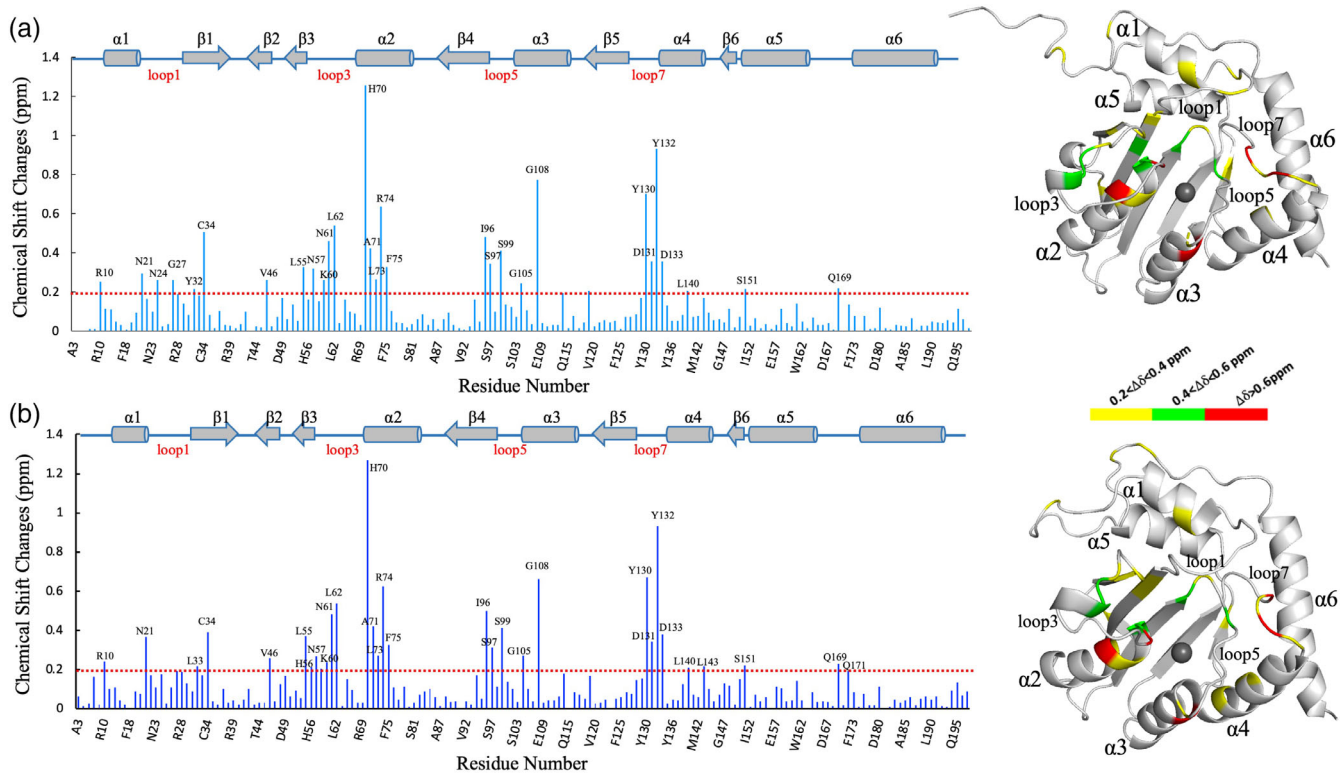

FIGURE 2 The chemical shift changes of backbone amide nitrogen and protons in two DNA-bound states of A3A$_{4M}$ compared to free A3A$_{4M}$. (a) DNA specifically bound A3A$_{4M}$. (b) DNA nonspecifically bound A3A$_{4M}$. In the left of (a, b), the secondary regions were labeled and drawn above the bar charts. The dashed lines indicated the lowest values, below which the chemical shift changes were not considered. In the right of (a, b), the residues in the surface of A3A$_{4M}$ structure with different scales (0.2–0.4 ppm, 0.4–0.6 ppm and >0.6 ppm) of the chemical shift changes were displayed in yellow, green and red, respectively

listed in Tables S1 and S2), 184 phi and 185 psi dihedral angel constrains based on the chemical shifts of backbone atoms of $A3A_{4M}$, 174 hydrogen-bond constraints based on the secondary structure of $A3A_{4M}$, as shown in Table S3. Constraints between the ligated residues (His^{70}, Cys^{101} and Cys^{106}) in the protein and the zinc ion were added using the procedure of Neuhaus et al as described previously.[35,36] The final two ensembles, each of which contained 20 structures of $A3A_{4M}$-DNA complexes with the lowest energies, were displayed in Figure 3a,b, with RMSD values of 0.55 ± 0.11 Å and 0.54 ± 0.07 Å for backbone atoms in the secondary structural regions, respectively, upon overlapping the backbone atoms at the secondary regions of $A3A_{4M}$. The Ramachandran plot displayed 89.0 and 86.6% of the residues in the most-favored regions, and no residues (0%) located in the disallowed regions, indicating that all structures were reasonable. On the whole, as shown in Figure 3c,d, the TC DNA mainly bound in a groove between loop 1 or 3 and loop 5 or 7, consistent with the NMR titration results, indicating the roles of these loops in the interactions between $A3A_{4M}$ and DNA. The global folding of $A3A_{4M}$ is almost identical in two bound states with an RMSD value of 1.27 Å upon 162 Cα atoms of the residues in the secondary structures. The loops 1, 3, 5 and 7 display plasticity to accommodate the conformational changes of the DNA upon its binding to $A3A_{4M}$.

To verify the effects of these loops on enhancing DNA binding, we varied the length of ssDNA (containing only one target motif TC) by cutting off or adding bases at either 5′- end or 3′- end, respectively, from TTC-1 to TTC-11 (Table 1 and Figure S6). Without adenine adjacent to TC motif at its 3′- end (i.e., TCA motif in TC DNA), all these DNA strands had dramatically decreased binding affinities to $A3A_{4M}$, compared to TC DNA. Compared to TTC-2 (containing 9 bases in total), $A3A_{4M}$ demonstrated no significant changes in binding affinities (all $K_D < 5$ μM) to TTC-3 (11 bases in total, adding 2 dT bases at 3′- end), TTC-4 (13 bases in total, adding 4 dT bases at 3′- end), TTC-5 (15 bases in total, adding 6 dT bases at 3′- end) and TTC-6 (17 bases in total, adding 8 dT bases at 3′- end). Since 3′- end bases of DNA mainly interacted with loops 1, 3, 5 and 7 of $A3A_{4m}$, as shown in Figure 3, this observation implied the indispensable roles of these loops in stabilizing the conformation of A3A-DNA complex. In contrast, compared to TTC-2, when the length of DNA was extended by adding different numbers of dT into 5′- end, the binding affinities (20 μM $< K_D <$ 40 μM) of TTC-8 (13 bases in total, adding 4 dT bases at 5′- end), TTC-9 (15 bases in total, adding 6 dT bases at 5′- end), TTC-10 (17 bases in total, adding 8 dT bases at 5′- end) and TTC-11 (21 bases in total, adding 12 bases at 5′- end) were remarkably impaired by 5–10 fold. This finding indicated that, the DNA strands, with larger number of flanking nucleotides at 5′- end than TTC-2, obviously weakened the interactions between $A3A_{4M}$ and DNA, and the conformation of DNA became more flexible in A3A-DNA complex. Meanwhile, TTC-7 DNA (11 bases in total, adding 2 dT bases at 5′- end) displayed binding affinity to $A3A_{4M}$ stronger binding affinities than TTC-1

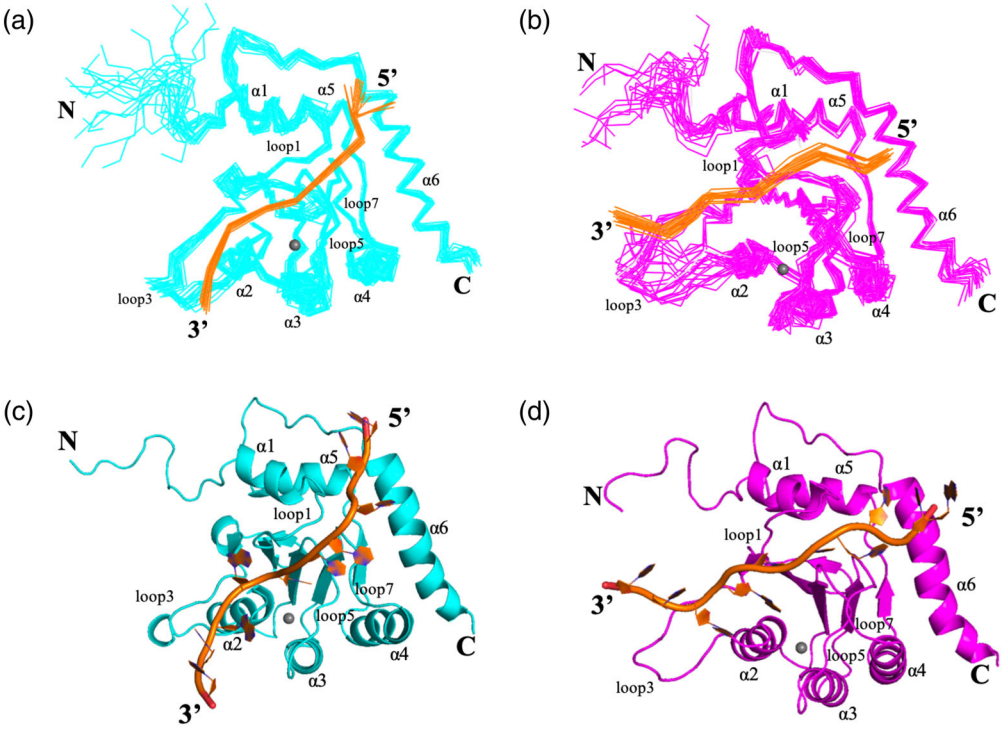

FIGURE 3 NMR structures of A3A-TC DNA complexes. (a) The bundle of 20 structures of $A3A^S$-DNA^S complex with the lowest energies. (b) The bundle of 20 structures of $A3A^{NS}$-DNA^{NS} complex with the lowest energies. (c) One structure of $A3A^S$-DNA^S complex. (d) One structure of $A3A^{NS}$-DNA^{NS} complex. In (a, b) and (c, d), DNA (in orange) and $A3A_{4M}$ (in cyan or pink) were displayed in ribbon and cartoon modes, respectively. The N- and C-termini, the loops 1, 3, 5 and 7, the helices α1, α2, α3, α4, α5 and α6 of $A3A_{4M}$, and 5′- and 3′- ends of DNA were labeled, respectively. The grey balls represented zinc ions

DNA (7 bases in total) (Figure S6a), and in an almost similar order of magnitude to those of TTC-2 DNA (9 bases in total) and TTC-3 DNA (11 bases in total) (Figure S6b), further implying that DNA with a length of 9–11 bases was most suitable for $A3A_{4M}$ interaction, consistent with the previous report.[34]

In $A3A^S$-DNA^S complex structure, the zinc ion coordinated with residues His^{70}, Cys^{101}, Cys^{106}, the whole DNA interacted with $A3A_{4M}$ also in a U-shaped manner. The target base dC_0 extended into the pocket of zinc ion binding site (Figure 4a,b), and had parallel or T-shaped π–π stacking interactions with the aromatic side-chains of the conserved residues His^{70} and Tyr^{130} (Figure 4a,c), respectively, similar to those observed in the reported structures of A3-DNA complexes (Figure 4d–f).[31–33] The conformation of dC_0 was stabilized by several hydrogen-bonds between Ala^{71} backbone NH and dC_0 O_2 atoms, between the carbonyl oxygen atoms of Trp^{98} and Ser^{99} and NH_2 of dC_0, and between the hydroxyl group of the side-chain of Thr^{31} and O_3 atom of the sugar ring of dC_0, which also addressed the specificity for dC_0 over dT_{-1} (Figure 4a). The base dT_{-1} was identified by the conserved residue Asp^{131} in loop 7 through hydrogen-bond between amide nitrogen of Asp^{131} and oxygen of dT_{-1} (Figure S7a,e). Identical to those observed in the crystal structures of A3A-DNA complex,[32,33] A3Bctd*-DNA complex[33] and A3G-CTD2*-DNA complex[31] (Figure S7b–d), the Asp^{131} side chain had a salt bridge to the side-chain of the conserved residue Arg^{189} in helix α6, which might enhance all hydrogen-bond interactions between loop 7 and base dT_{-1}. Similarly, as shown in Figure S8, the conserved residue His^{29} in loop 1 had π–π stacking interactions with dA_{+1}, as reported in the crystal structures of A3A-DNA,[32] A3Bctd*-DNA[33] and A3G-CTD2*-DNA[31] complexes, which once again confirmed that residue His^{29} might work as "latch" in the process of A3A recognizing the TCA motif in the substrate DNA.

2.3 | $A3A^{NS}$-DNA^{NS} structure implies three new sites important to DNA binding

In $A3A^{NS}$-DNA^{NS} complex structure (Figure 5a), DNA^{NS} located in a region almost similar to that observed in the structure of $A3A^S$-DNA^S complex. However, the target base dC_0 did not extend into the zinc ion binding pocket. The averaged distances between zinc ion and N4 atom of dC_0 in all final 20 structures were measured as 12.0 Å, which was much farther than that (5.0 Å) in all final 20 structures of $A3A^S$-DNA^S complex. Therefore, we

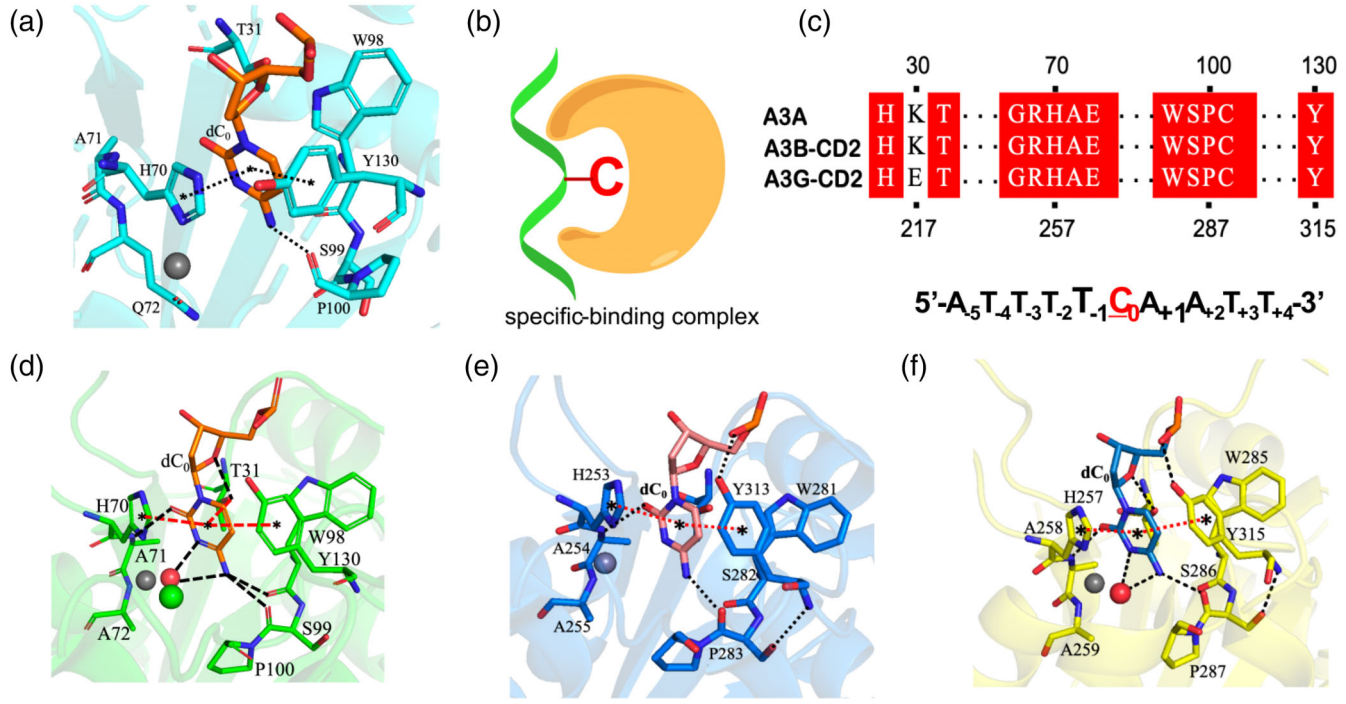

FIGURE 4 Structural analysis of $A3A^S$-DNA^S complex. (a) The target dC_0 identified by A3 members in structures of $A3A^S$-DNA^S complex. (b) The specific binding complex displayed in a cartoon mode, where dC_0 inserted into zinc-ion binding center. (c) Conserved residues among A3A, A3B and A3G interact with dC_0. (d) The target dC_0 identified by A3 members in structures of A3A-DNA complex (5KEG). (e) The target dC_0 identified by A3 members in structures of A3Bctd*-DNA complex (5TD5), and (f) A3G-CTD2* complex (6BUX). The dashed lines with stars in both ends indicate stacking interactions. The dash lines without stars in both ends imply hydrogen-bonds

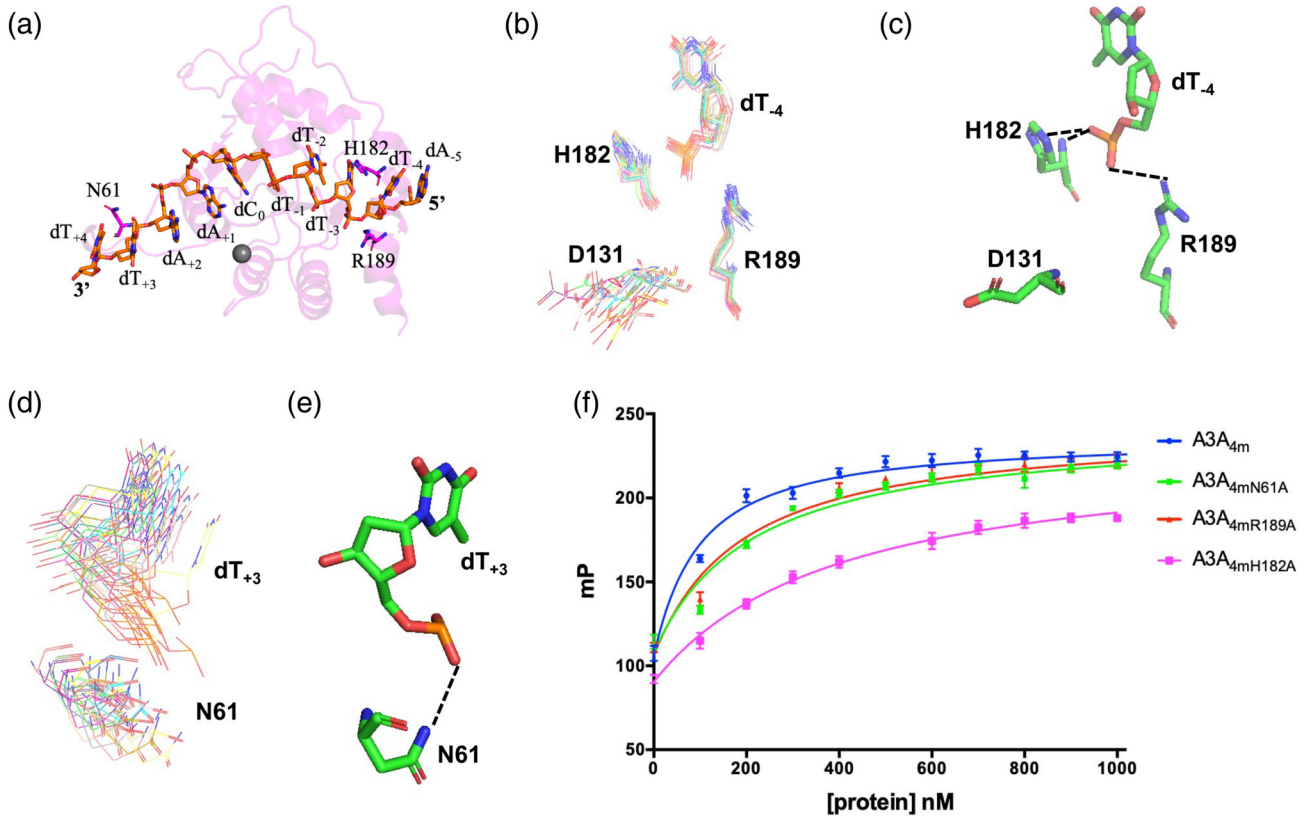

FIGURE 5 The NMR structure of $A3A^{NS}$-DNA^{NS} complex indicated three new sites important to DNA binding. (a) The positions of residues N61, H182 and R189. DNA was displayed in stick mode, $A3A_{4M}$ was shown in transparent, pink cartoon mode. (b, c) Residues H182 and R189 formed H-bonds with DNA base dT_{-4}. (d, e) Residue N61 formed H-bond with dT_{+3} . In (b, d), the residues N61, D131, H182 and R189 in $A3A_{4M}$ and bases dT_{+3} and dT_{-4} in DNA were shown in line mode in all final 20 structures with the lowest energies, indicating the convergent orientations of their side-chains. H182 located in regid α6 helix, while N61 was in flexible loop 3, which resulted in convergent conformation of H182, and shifted-conformation of N61. In (c, e), residues N61, D131, H182 and R189 in A3A and bases dT_{-4} and dT_{+3} in DNA were shown in stick mode. The dashed lines represented H-bonds. (f) The binding affinities of $A3A_{4M}$ and its variants to TC DNA were measured by fluorescent polarization assay

thought that this kind of interaction between $A3A^{NS}$ and DNA^{NS} was nonspecific, however, which was not single one case reported between DNA and A3 family members. For examples, as displayed in Figure S9, poly-dT DNA interactions with rA3G-CD1 only led to the conformational change of the loops and residues surrounding the Zn^{2+}-coordinated center.[29] The hA3F-CD2 bound to poly-dT DNA through a positively charged site distal to the active zinc ion binding center.[27] DNA (containing two TC motifs at both ends) interacted with hA3Fc-CD2 dimer at two sites existing in the hA3Fc-CD2 monomers.[28] In all these structures, as well as that of $A3A^{NS}$-DNA^{NS} complex, the target dC_0 was not in the zinc ion binding pocket. However, obviously, DNA bound to different regions of A3 proteins, suggesting that nonspecific interactions between DNA and A3 members were in varied manners.

Structural analysis on $A3A^{NS}$-DNA^{NS} complex showed that the backbone phosphate ions of base dT_{-4} at 5′- end and of base dT_{+3} at 3′- end formed hydrogen-bonds with the side-chains of the residues Asn61, His182 and Arg189 (Figure 5b–e), respectively. This observation explained why the chemical shifts of backbone atoms of residues His182 and Arg189 did not change (Figure 2b) upon DNA nonspecifically interacting with $A3A_{4M}$. At the same time, the side-chain of Asp131 did not have a salt-bridge with the side-chain of residue Arg189, different from the observation in structure of $A3A^{S}$-DNA^{S} complex (Figure S7a,b). To confirm whether these three H-bonds stabilized the conformation of $A3A^{NS}$-DNA^{NS} complex, we replaced them into alanine, and measured the binding affinities of these $A3A_{4M}$ variants to TC DNA (Figure 5f). Their binding affinities were decreased by 2–4.5 folds, compared to $A3A_{4M}$. Thus, $A3A^{NS}$-DNA^{NS} structure explored three key sites useful for A3A interaction with DNA.

3 | CONCLUSIONS

In this report, we determined two solution structures of $A3A_{4M}$ in complexes with TC DNA in specific and

nonspecific binding ways, respectively. The nonspecific binding mode of $A3A_{4M}$ to ssDNA is not unique. Previously, the catalytic domain of APOBEC3B (i.e., A3B-CTD) was suggested to specifically identify target base dC_0 by sliding along ssDNA (i.e., nonspecific interaction with ssDNA).[37] A3B slides only for a relatively short distance and tends to dissociate from the ssDNA before reaching the target sequence. The full-length A3G (i.e., FL-A3G, containing inactive A3G-NTD and active A3G-CTD domains) has higher deaminase activity than A3G-CTD. FL-A3G interacts with ssDNA in specific and nonspecific modes, in which A3G displayed elevated affinity for specific sequence ssDNA than for nonspecific sequence ssDNA.[38] A3G-NTD interacts with ssDNA in a nonspecific mode, while A3G-CTD interacts with ssDNA in a specific mode. Both domains of A3G contribute to the sequence specific binding of ssDNA. To identify target motif 5′-CC-3′, A3G first binds to ssDNA in a sequence nonspecific manner and slides along the ssDNA without directional preference.[39] Similar to A3B and A3G, before the target base dC_0 in TC motif was specifically identified, A3A must slide along ssDNA through nonspecific interaction with ssDNA. Thus, the nonspecific interaction between A3A and ssDNA plays a role in guiding substrate DNA to be specifically recognized by the active center of A3A. This not only revealed that A3s had multiple nonspecific recognition manners for substrate ssDNA, but also provide implications of how A3s deaminate ssDNA in solution.

4 | MATERIALS AND METHODS

4.1 | Supplemental methods and materials

4.1.1 | Expression and purification of $A3A_{4M}$

The gene of $A3A_{4M}$ or its variants was cloned into the region between *BamH*I and *Xho*I cleavage sites of a recombined pGEX-6p-1 plasmid which contained an His_6-tag adjacent to the N-terminal GST tag, and HRV 3c cleavage site. $A3A_{4M}$ and its variants were expressed in BL-21(DE3) *Escherichia coli* cells. Cell cultures were grown to OD_{600} value equal to about 0.8 and induced with a final concentration of 0.4 mM IPTG for 20 hr at 16°C. Cells were re-suspended in Ni^{2+}-binding buffer A (50 mM Tris–HCl pH 7.5, 300 mM NaCl, 50 μM $ZnCl_2$ and 10 mM β-mercaptoethanol [β-ME]) with protease inhibitor (PMSF) and lysed at 15 kpsi using a hydraulic cell disruption system (Constant System JINBO Benchtop) (Guangzhou Juneng Biology and Technology Co., Ltd., Guangzhou, China). The lysate was centrifuged at 12,000 rpm and 4°C for 55 min to remove cellular debris prior to loading into a Ni-NTA resin (GE Health). The column was washed with 10 column volumes buffer A (50 mM Tris–HCl pH 7.5, 300 mM NaCl, 50 μM $ZnCl_2$ and 10 mM β-ME) followed by 10 volumes buffer B (50 mM Tris–HCl pH 7.5, 300 mM NaCl, 20 mM imidazole, 50 μM $ZnCl_2$ and 10 mM β-ME). The bound protein was eluted with 10 column volumes of buffer C (50 mM Tris–HCl pH 7.5, 300 mM NaCl, 20 mM imidazole, 50 μM $ZnCl_2$ and 10 mM β-ME). The elute was then dialyzed with buffer D (25 mM Na_2HPO_4 pH 7.3, 200 mM NaCl, 50 μM $ZnCl_2$ and 5 mM DTT). Fractions containing $A3A_{4M}$ were then concentrated and purified on a Superdex75 16/300 GL column (GE Health) previously equilibrated with buffer D (25 mM Na_2HPO_4 pH 7.3, 200 mM NaCl, 50 μM $ZnCl_2$ and 5 mM DTT).

4.2 | DNA synthesis and purification

All DNA strands with or without FAM label were commercially synthesized from Shanghai Biosune Biotech Co., Ltd., China at a PAGE grade. The molecular weight of all strands was confirmed by running PAGE gel and MALDI TOF mass spectroscopy.

4.3 | Fluorescence polarization

To determine the binding affinities of $A3A_{4M}$ and its variants to different DNA strands, or 5′-fluoresceinated DNA strands were commercially synthesized at a HPLC grade (Shanghai Sangon Biotech Co., Ltd., China) with the corresponding sequences. The fluorescence polarization (FP) was performed, where all proteins were diluted in buffer D (25 mM Na_2HPO_4 pH 7.3, 200 mM NaCl, 50 μM $ZnCl_2$ and 5 mM DTT) for FP and incubated with a 10 nM 5′- end 6-FAM-labeled ssDNA at room temperature in a total reaction volume of 200 μL. FP assay was measured at 25°C using SpectraMax i3x Platform (Molecular Devices, Inc.) with 490 nm excitation and 535 nm emission wavelengths, respectively. The dissociation constants (K_D) were determined by a nonlinear least-squares analysis using the program Prism 5 (GraphPad, Inc.). Data shown are averaged values of three repeated measurements.

4.4 | NMR data collection and spectra analysis

To correctly assign NMR signals of DNA used in the structural determination of A3A-DNA complex, we first performed NMR experiments on DNA samples of TC

DNA, CC DNA, TU DNA and TT DNA. All DNA samples were about 1 mM dissolved in buffer containing 25 mM Na_2HPO_4 pH 7.3, 200 mM NaCl, 50 μM $ZnCl_2$, 5 mM DTT, 100% D_2O. All NMR samples were placed in 5-mm Shigemi NMR tubes. All NMR experiments were performed on a Varian Unity Inova 600 NMR spectrometer (with cryo-probe) equipped with triple resonances and pulsed field gradients. Two-dimensional (2D) ^1H-^1H NOESY (with a mixing time of 250 ms), TOCSY (with a mixing time of 80 ms), and DQF-COSY spectra were acquired at 20°C using a spectral width of 6,100 Hz in both dimensions. The acquisition data points were set to 2048 × 512 (complex points). The watergate sequence was used for water suppression. During data processing, the 45° or 60° shifted sine-squared functions were applied to NOESY and TOCSY spectra. The fifth-order polynomial functions were employed for the baseline corrections. The final spectral sizes are 2,048 × 1,024. The ^{31}P NMR spectra were collected at about 1.5 mM concentration in D_2O (25 mM Na_2HPO_4 pH 7.3, 200 mM NaCl, 50 μM $ZnCl_2$ and 5 mM dithiothreitol-d_{10} [d_{10}-DTT]) at 20°C at 600 MHz Varian spectrometer including the one dimensional proton-decoupled phosphorus spectrum, and 2D heteronuclear ^{31}P-^1H Correlation Spectroscopy (^{31}P-^1H HETCOR). Assignments of the individual ^{31}P resonance were accomplished by a combination of 2D ^1H-^1H NOESY, COSY, TOCSY and ^{31}P-^1H HETCOR spectra.

To determine NMR structure of $A3A_{4M}$ in complex with TC DNA, 0.25 mM uniformly ^{15}N-/^{13}C double isotope labeled or ^{15}N-/^{13}C-/70% ^2H triple labeled $A3A_{4M}$ plus 0.5 mM unlabeled TC DNA was prepared in NMR buffer (25 mM Na_2HPO_4 pH 7.3, 200 mM NaCl, 50 μM $ZnCl_2$ and 5 mM d_{10}-DTT) containing 10% or 100% D_2O. All NMR experiments were performed at 20°C on a Varian Unity Inova or Agilent 600 NMR spectrometer (with cryo-probe) equipped with triple resonances and pulsed field gradients, or on Bruker Avance or Agilent III-800MHz, 850MHz, 900MHz NMR spectrometers (with cryo-probe) equipped with four channels and z-axis pulsed-field gradient.

The standard suite of experiments were acquired for assigning the ^1H, ^{13}C and ^{15}N backbone and side-chain chemical shifts of ^{13}C and ^{15}N double labeled $A3A_{4M}$ in complex with unlabeled DNA, and for the collection of NOE-based distance restraints were measured,[40,41] including the 2D ^{13}C-edited HSQC in both aliphatic and aromatic regions, and ^{15}N-edited HSQC; the three-dimensional (3D) HNCA, HNCO, HN(CO)CA, HNCACB, CBCA(CO)NH, ^{15}N-resolved HSQC-TOCSY, HCCH-TOCSY in both aliphatic and aromatic regions, ^{15}N-resolved HSQC-NOESY, ^{13}C-resolved HSQC-NOESY for both aliphatic and aromatic resonances, 2D $(H_\beta)C_\beta(C_\gamma C_\delta)H_\delta$ and $(H_\beta)C_\beta(C_\gamma C_\delta C_\varepsilon)H_\varepsilon$ spectra for correlation of C_β and H_δ or H_ε in aromatic rings used in aromatic protons assignment.[42] To obtain NMR signals of bound TC DNA, 2D ^{13}C/^{15}N filtered ^1H-^1H TOCSY, NOESY spectra and 2D ^{31}P-^1H HETCOR spectra were collected. The intermolecular NOEs between ^{13}C-/^{15}N-labeled $A3A_{4M}$ and unlabeled TC DNA were obtained by analyzing 3D ^{13}C-F1 edited, ^{13}C/^{15}N-F3 filtered NOESY spectra.

All NMR spectra were processed with the program NMRPipe[43] and analyzed with Sparky 3 software.[44] The ^1H chemical shifts were referenced to 2, 2-dimethylsilapentane-5-sulfonic acid (DSS), the ^{13}C- and ^{15}N-resonances were indirectly referenced to DSS, and the ^{31}P chemical shifts were referenced to an external standard of 85% H_3PO_4.

4.5 | Analysis of ultracentrifugation experiments

Sedimentation velocity experiments were performed on a Beckman XL-I analytical ultracentrifuge equipped with an eight-cell rotor under 42,000 rpm at 20°C. The partial specific volume of different samples and the buffer density were calculated using the program SEDNTERP (http://www.rasmb.bbri.org/). The final sedimentation velocity data were analyzed and fitted to a continuous sedimentation coefficient distribution model using the program SEDFIT. The fitting results were further output to the Origin 9.0 software and aligned with each other.

4.6 | NMR structure determination

The structural calculations of the $A3A^S$-DNA^S and $A3A^{NS}$-DNA^{NS} complexes were carried out using a standard simulated annealing protocol implemented in the program XPLOR-2.37 (NIH version).[45] 3,409 and 3,346 distance constraints derived from NOE intensities were classified into 1.8–2.9 Å, 1.8–3.5 Å, 1.8–5.0 Å groups, corresponding to strong, medium and weak NOEs, respectively, while intermolecular distance restrains were sorted into weak (1.8–5.0 Å) and very weak (1.8–6.0 Å) groups. 184 phi and 185 psi dihedral angles were derived from the chemical shifts of the backbone atoms (HN, HA, CO, CA) by the program TALOS.[43,46] One hundred and seventy-four hydrogen-bond restraints for secondary structures were generated by analyzing secondary structural regions in the reported free NMR and X-ray apo-A3A structures[47–50] for the final structure calculation. Constraints between the protein ligands and the zinc ion were added using the procedure of Neuhaus et al as described previously.[35,36] A total of 10 iterations

(50 structures in the initial 10 iterations) were performed. One hundred structures were computed in the last five iterations, 20 conformers with the lowest energy are used to represent the 3D structures. In the ensemble of the simulated annealing 20 structures, there was no distance constraint violation more than 0.3 Å and no torsion angle violation more than 5°. The final 20 structures of the complex A3A with different DNA with lowest energy were evaluated with the program PROCHECK-NMR and PROCHECK.[51] All figures related to structures were generated using the program PyMOL.

ACKNOWLEDGMENTS

This work was supported by National Program on Key Basic Research Project of China (2017YFE0108200 and 2016YFA0502302), by National Science Foundation of China (NSFC) under No. 91753119, 21977110, 21778065 and 21807105, by the Strategic Priority Research Program of the Chinese Academy of Sciences (XDB 20000000) and by Center for Excellence in Molecular Synthesis, CAS (FZHCZY020600). The authors sincerely thank facility team members in National Center of Protein Sciences Shanghai (NCPSS), in State Key Laboratory of Magnetic Resonance and Atomic Molecular Physics, Wuhan Institute of Physics and Mathematics, Chinese Academy of Sciences (CAS), the NMR center of Shanghai Institute of Materia Medica, CAS, in High Magnetic Field Laboratory (HMFL), CAS, for their great help with NMR spectra data acquirement. The atom coordinates of NMR structures were deposited into protein data bank (RCSB) with access codes 7D3X ($A3A^{S}$-DNA^{S}) and 7D3W ($A3A^{NS}$-DNA^{NS}), the NMR chemical shifts of TC DNA strand and specifically and nonspecifically DNA-bound $A3A_{4M}$ were deposited into BMRB with access numbers 36389 ($A3A^{S}$-DNA^{S}) and 36388 ($A3A^{NS}$-DNA^{NS}).

AUTHOR CONTRIBUTIONS

Yaping Liu: Data curation (equal); formal analysis (equal); investigation (supporting); validation (equal). **Wenxian Lan:** Methodology (equal); software (equal); validation (equal). **Chunxi Wang:** Data curation (equal); software (equal); supervision (equal); validation (equal). **Chunyang Cao:** Conceptualization (equal); funding acquisition (lead); project administration (lead); supervision (lead).

CONFLICT OF INTEREST

The authors declare no potential conflict of interest.

ORCID

Chunyang Cao https://orcid.org/0000-0001-7865-8249

REFERENCES

1. Yu Q, Konig R, Pillai S, et al. Single-strand specificity of APOBEC3G accounts for minus-strand deamination of the HIV genome. Nat Struct Mol Biol. 2004;11:435–442.
2. Mangeat B, Turelli P, Caron G, Friedli M, Perrin L, Trono D. Broad antiretroviral defence by human APOBEC3G through lethal editing of nascent reverse transcripts. Nature. 2003;424:99–103.
3. Zhang H, Yang B, Pomerantz RJ, Zhang C, Arunachalam SC, Gao L. The cytidine deaminase CEM15 induces hypermutation in newly synthesized HIV-1 DNA. Nature. 2003;424:94–98.
4. Lada AG, Dhar A, Boissy RJ, et al. AID/APOBEC cytosine deaminase induces genome-wide kataegis. Biol Direct. 2012;7:47.
5. Chelico L, Sacho EJ, Erie DA, Goodman MF. A model for oligomeric regulation of APOBEC3G cytosine deaminase-dependent restriction of HIV. J Biol Chem. 2008;283:13780–13791.
6. Chelico L, Pham P, Calabrese P, Goodman MF. APOBEC3G DNA deaminase acts processively 3′–>5′ on single-stranded DNA. Nat Struct Mol Biol. 2006;13:392–399.
7. Rausch JW, Chelico L, Goodman MF, Le Grice SF. Dissecting APOBEC3G substrate specificity by nucleoside analog interference. J Biol Chem. 2009;284:7047–7058.
8. Yang H, Ito F, Wolfe AD, et al. Understanding the structural basis of HIV-1 restriction by the full length double-domain APOBEC3G. Nat Commun. 2020;11:632.
9. Sheehy AM, Gaddis NC, Choi JD, Malim MH. Isolation of a human gene that inhibits HIV-1 infection and is suppressed by the viral Vif protein. Nature. 2002;418:646–650.
10. Olson ME, Harris RS, Harki DA. APOBEC enzymes as targets for virus and cancer therapy. Cell Chem Biol. 2018;25:36–49.
11. Venkatesan S, Rosenthal R, Kanu N, et al. Perspective: APOBEC mutagenesis in drug resistance and immune escape in HIV and cancer evolution. Ann Oncol. 2018;29:563–572.
12. Ran X, Ao Z, Yao X. Apobec3G-based strategies to defeat HIV infection. Curr HIV Res. 2016;14:217–224.
13. Goila-Gaur R, Strebel K. HIV-1 Vif, APOBEC, and intrinsic immunity. Retrovirology. 2008;5:51.
14. Zhang WY, Du J, Evans SL, Yu YK, Yu XF. T-cell differentiation factor CBF-beta regulates HIV-1 Vif-mediated evasion of host restriction. Nature. 2012;481:376–379.
15. Jäger S, Kim DY, Hultquist JF, et al. Vif hijacks CBF-beta to degrade APOBEC3G and promote HIV-1 infection. Nature. 2012;481:371–375.
16. Marin M, Rose KM, Kozak SL, Kabat D. HIV-1 Vif protein binds the editing enzyme APOBEC3G and induces its degradation. Nat Med. 2003;9:1398–1403.
17. Sheehy AM, Gaddis NC, Malim MH. The antiretroviral enzyme APOBEC3G is degraded by the proteasome in response to HIV-1 Vif. Nat Med. 2003;9:1404–1407.
18. Yu X, Yu Y, Liu B, et al. Induction of APOBEC3G ubiquitination and degradation by an HIV-1 Vif-Cul5-SCF complex. Science. 2003;302:1056–1060.
19. Lecossier D, Bouchonnet F, Clavel F, Hance AJ. Hypermutation of HIV-1 DNA in the absence of the Vif protein. Science. 2003;300:1112.
20. Berger G, Durand S, Fargier G, et al. APOBEC3A is a specific inhibitor of the early phases of HIV-1 infection in myeloid cells. PLoS Path. 2011;7:e1002221.
21. Taura M, Song E, Ho YC, Iwasaki A. Apobec3A maintains HIV-1 latency through recruitment of epigenetic silencing

machinery to the long terminal repeat. Proc Natl Acad Sci U S A. 2019;116:2282–2289.
22. Warren CJ, Xu T, Guo K, et al. APOBEC3A functions as a restriction factor of human papillomavirus. J Virol. 2015;89:688–702.
23. Nakaya Y, Stavrou S, Blouch K, Tattersall P, Ross SR. In vivo examination of mouse APOBEC3- and human APOBEC3A- and APOBEC3G-mediated restriction of parvovirus and herpesvirus infection in mouse models. J Virol. 2016;90:8005–8012.
24. Suspene R, Aynaud MM, Koch S, et al. Genetic editing of herpes simplex virus 1 and Epstein-Barr herpesvirus genomes by human APOBEC3 cytidine deaminases in culture and in vivo. J Virol. 2011;85:7594–7602.
25. Jin JY, Yan XY, Liu YP, Lan WX, Wang CX, Xu B, & Cao, CY. Recent advances in the structural studies on cytosine deaminase APOBEC3 family members and their nucleic acid complexes. Acta Chim Sinica. 2019;77:1089–1098.
26. Salter JD, Smith HC. Modeling the embrace of a mutator: APOBEC selection of nucleic acid ligands. Trends Biochem Sci. 2018;43:606–622.
27. Fang Y, Xiao X, Li SX, Wolfe A, Chen XS. Molecular interactions of a DNA modifying enzyme APOBEC3F catalytic domain with a single-stranded DNA. J Mol Biol. 2018;430:87–101.
28. Cheng C, Zhang TL, Wang CX, Lan WX, Ding JP, Cao CY. Crystal structure of cytidine deaminase human APOBEC3F chimeric catalytic domain in complex with DNA. Chinese J Chem. 2018;36:1241–1248.
29. Xiao X, Li SX, Yang H, Chen XS. Crystal structures of APOBEC3G N-domain alone and its complex with DNA. Nat Commun. 2016;7:12193.
30. Yan XX, Lan W, Wang CX, Cao C. Structural investigations on the interactions between cytidine deaminase human APOBEC3G and DNA. Chem Asian J. 2019;14:2235–2241.
31. Maiti A, Myint W, Kanai T, et al. Crystal structure of the catalytic domain of HIV-1 restriction factor APOBEC3G in complex with ssDNA. Nat Commun. 2018;9:2460.
32. Kouno T, Silvas TV, Hilbert BJ, et al. Crystal structure of APOBEC3A bound to single-stranded DNA reveals structural basis for cytidine deamination and specificity. Nat Commun. 2017;8:15024.
33. Shi K, Carpenter MA, Banerjee S, et al. Structural basis for targeted DNA cytosine deamination and mutagenesis by APOBEC3A and APOBEC3B. Nat Struct Mol Biol. 2017;24:131–139.
34. Byeon IJ, Ahn J, Mitra M, et al. NMR structure of human restriction factor APOBEC3A reveals substrate binding and enzyme specificity. Nat Commun. 2013;4:1890.
35. Neuhaus D, Nakaseko Y, Schwabe JW, Klug A. Solution structures of two zinc-finger domains from SWI5 obtained using two-dimensional 1H nuclear magnetic resonance spectroscopy. A zinc-finger structure with a third strand of beta-sheet. J Mol Biol. 1992;228:637–651.
36. Kwon K, Cao C, Stivers JT. A novel zinc snap motif conveys structural stability to 3-methyladenine DNA glycosylase I. J Biol Chem. 2003;278:19442–19446.
37. Wan L, Nagata T, Morishita R, Takaori-Kondo A, Katahira M. Observation by real-time NMR and interpretation of length- and location-dependent deamination activity of APOBEC3B. ACS Chem Biol. 2017;12:2704–2708.
38. Shlyakhtenko LS, Dutta S, Banga J, Li M, Harris RS, Lyubchenko YL. APOBEC3G interacts with ssDNA by two modes: AFM studies. Sci Rep. 2015;5:15648.
39. Kamba K, Nagata T, Katahira M. Catalytic analysis of APOBEC3G involving real-time NMR spectroscopy reveals nucleic acid determinants for deamination. PloS One. 2015;10:e0124142.
40. Bax A, Grzesiek S. Methodological sdvances in protein NMR. Acc Chem Res. 1993;26:131–138.
41. Clore GM, Gronenborn AM. Determining the structures of large proteins and protein complexes by NMR. Trends Biotechnol. 1998;16:22–34.
42. Yamazaki T, Forman JD, Kay LE. 2-Dimensional NMR experiments for correlating C-13-Beta and H-1-Delta/Epsilon chemical-shifts of aromatic residues in C-13-labeled proteins via scalar couplings. J Am Chem Soc. 1993;115:11054–11055.
43. Delaglio F, Grzesiek S, Vuister GW, Zhu G, Pfeifer J, Bax A. NMRPipe: A multidimensional spectral processing system based on UNIX pipes. J Biomol NMR. 1995;6:277–293.
44. Goddard TD, Kneller DG. SPARKY 3. San Francisco, CA: University of California, 2001.
45. Kuszewski J, Clore GM. Sources of and solutions to problems in the refinement of protein NMR structures against torsion angle potentials of mean force. J Magn Reson. 2000;146:249–254.
46. Cornilescu G, Delaglio F, Bax A. Protein backbone angle restraints from searching a database for chemical shift and sequence homology. J Biomol NMR. 1999;13:289–302.
47. Chen KM, Harjes E, Gross PJ, et al. Structure of the DNA deaminase domain of the HIV-1 restriction factor APOBEC3G. Nature. 2008;452:116–119.
48. Furukawa A, Nagata T, Matsugami A, et al. Structure, interaction and real-time monitoring of the enzymatic reaction of wild-type APOBEC3G. EMBO J. 2009;28:440–451.
49. Holden LG, Prochnow C, Chang YP, et al. Crystal structure of the anti-viral APOBEC3G catalytic domain and functional implications. Nature. 2008;456:121–124.
50. Lu X, Zhang T, Xu Z, et al. Crystal structure of DNA cytidine deaminase ABOBEC3G catalytic deamination domain suggests a binding mode of full-length enzyme to single-stranded DNA. J Biol Chem. 2015;290:4010–4021.
51. Laskowski RA, Rullmannn JA, MacArthur MW, Kaptein R, Thornton JM. AQUA and PROCHECK-NMR: Programs for checking the quality of protein structures solved by NMR. J Biomol NMR. 1996;8:477–486.

SUPPORTING INFORMATION

Additional supporting information may be found in the online version of the article at the publisher's website.

How to cite this article: Liu Y, Lan W, Wang C, Cao C. Two different kinds of interaction modes of deaminase APOBEC3A with single-stranded DNA in solution detected by nuclear magnetic resonance. Protein Science. 2022;31:443–53. https://doi.org/10.1002/pro.4242